International Journal of Heat and Mass Transfer 52 (2009) 751–759

Contents lists available at ScienceDirect

International Journal of Heat and Mass Transfer

journal homepage: www.elsevier.com/locate/ijhmt

Coupled heat and mass transfer through asymmetric porous membranes with finger-like macrovoids structure

Li-Zhi Zhang *

Key Laboratory of Enhanced Heat Transfer and Energy Conservation of Education Ministry, School of Chemical and Energy Engineering, South China University of Technology, Guangzhou 510640, China

ARTICLE INFO

Article history:
Received 12 December 2007
Received in revised form 14 July 2008
Available online 15 September 2008

Keywords:
Heat transfer
Mass transfer
Asymmetric membranes
Finger-like macrovoids

ABSTRACT

Asymmetric porous membranes with finger-like macrovoids have been extensively used in various processes, either directly as the transfer media or indirectly as the substrate for active layer. Heat and mass transfer through such membranes are the key parameters influencing system performance. However, previous studies on heat and mass transport only treated these membranes as a black box of homogeneous porous media by neglecting their asymmetric nature in structure, which fails to disclose the relations between the membrane structure and system performance. To solve this problem, this study gives a more detailed investigation of the thermal and mass diffusion through these membranes, with the help of scanning electron microscope (SEM) observations of membrane surface and cross-sectional structures. In the model setup, the whole membrane is classified into three layers: a sponge-like porous support layer, a layer of porous media with finger-like macrovoids, and a thin denser skin layer with smaller pores. The model is then incorporated into the analysis of coupled heat and mass transfer in a membrane exchanger for moisture permeations. Results show that the effective diffusivity of the membrane has been dramatically improved due to the existence of more than 70,000 per meter large finger-like voids inside.

1. Introduction

Porous membranes have been extensively used in various processes such as membrane distillation [1,2], pervaporation [3], gas separation [4], membrane reactors [5,6], fuel cells [7], and enthalpy recovery [8,9]. They are used either directly as the transfer media, or indirectly as the substrate support for the permselective active layer.

Phase-inversion method has been the widely used technology for membrane preparation since it was successfully used by Loeb and Sourirajan to develop cellulose acetate membranes for seawater desalination in 1960s [10]. According to this method, the formation of membrane structure is controlled by both the thermodynamics of the casting solution and the kinetics of transport process. Usually, depending on the rate of phase separation, two different structures, namely a symmetric sponge-like (from delayed phase demixing) or an asymmetric finger-like structure (from instantaneous phase demixing) can be expected [10–12]. Fig. 1 shows a typical symmetric sponge-like membrane structure and Fig. 2 shows a typical asymmetric finger-like structure. They are the scanning electron microscope (SEM) of the cross-sections of a polyether sulphone (PES) and a polyvinylidene fluoride (PVDF) membrane, respectively. Fig. 2 is actually an upside down graph of a real asymmetric membrane which is composed of three parts from bottom to top: a sponge-like porous support, a porous media with finger-like and nearly parallel macrovoids, and finally a very thin skin layer with rather small pores. This denser skin layer usually acts as the permselective active layer to separate substances. Due to the existence of large finger-like macrovoids, it is qualitatively believed that the asymmetric membranes have less resistance than symmetric membranes, and thus are beneficial for permeation performance. As a result, asymmetric membranes with finger-like macrovoids have been used more extensively than symmetric membranes [10–14].

Heat and mass transfer through the membranes are the key factors influencing system performance of various aforementioned membrane-related processes. Traditionally, the membranes were treated as a black box, by assuming them a homogeneous porous media and neglecting their structural non-uniformity in thickness [6–12]. The methodology is reasonable in that it is simple in modeling. However, it fails to predict the relations between the membrane structure and the heat mass transfer properties, especially for the widely used asymmetric membranes that have finger-like macrovoids.

In this study, coupled heat and mass transfer in a membrane exchanger in which two air streams exchange heat and moisture simultaneously is investigated. The unit simulates an air to air heat mass exchanger. Emphasis is on the detailed modeling of heat and mass transfer through the asymmetric membranes, based on the

* Tel./fax: +86 20 87114268.
E-mail address: Lzzhang@scut.edu.cn

0017-9310/$ - see front matter © 2008 Elsevier Ltd. All rights reserved.
doi:10.1016/j.ijheatmasstransfer.2008.07.029

Nomenclature

c_p	specific heat (kJ kg^{-1} K^{-1})
D	diffusivity (m^2/s)
D_h	hydrodynamic diameter (m)
d_p	pore diameter (m)
h	convective heat transfer coefficient (kW m^{-2}K^{-1})
$\dot{m}_v$	emission rate (kg m^{-2} s^{-1})
k	convective mass transfer coefficient (m/s)
l_f	finger void length (m)
Le	Lewis number
M	molecule weight (kg/mol)
NTU	number of transfer units
Nu	Nusselt number
n_f	number of finger voids (1/m)
P	Atmospheric pressure (Pa)
q	heat flux (kW m^{-2})
R	gas constant, 8.314 J/(mol K); resistance (s/m)
Sh	Sherwood number
T	temperature (K)
u_a	air bulk velocity (m/s)
v	molecular diffusion volume
x	coordinate (m)

Greek letters

ρ	density (kg/m^3)
λ	heat conductivity (W m^{-1} K^{-1})
ω	humidity ratio (kg moisture/kg air)
τ	pore tortuosity
ε	porosity
δ	thickness (μm)
α	skew angle (°)

Superscript

*	dimensionless

Subscripts

a	air
e	equivalent, exhaust air
f	finger, fresh air
i	inlet
k	Knudsen
m	membrane
o	outlet, ordinary
s	sensible, solid
tot	total
v	vapor

SEM observations of membrane surface and cross-sectional structures. The reason for an increased effective diffusivity with finger-like macrovoids will be quantitatively analyzed.

2. Experimental work

2.1. Test rig

An experimental setup has been built to study the simultaneous heat and moisture transport through an asymmetric porous membrane. The whole test rig is shown in Fig. 3. Ambient air is humidified and is driven to a heating/cooling coil in a hot/cool water bath. The cooling coil can also act as dehumidifier when necessary. After the temperature and humidity reach test conditions, the air is then sucked through the exchanger for heat and moisture exchange. This flow is denoted as the hot and humid fresh stream. Another flow is driven directly from ambient to the exchanger. It is denoted as the cool and dry exhaust flow. The membrane, which is developed in the laboratory, is sandwiched by two stainless steel rectangular shells. Two parallel rectangular air passages on both sides of membrane are formed, which is like a one-plate plate-and-shell heat exchanger. The flow is arranged in a counter flow configuration, to have maximum exchange effectiveness, as shown in Fig. 4. In the test, a 10 mm thick insulation layer is placed on the inner surface of the shell to prevent heat dissipation from the shell to the surroundings. Moisture dissipation from air stream to the surroundings is negligible. After the exchanger and pipes are installed, additional insulation is added on the outside surfaces to minimize heat losses from the unit. The PVDF made is highly hydrophobic, so the vapor condensation and blocking in the pores are prevented.

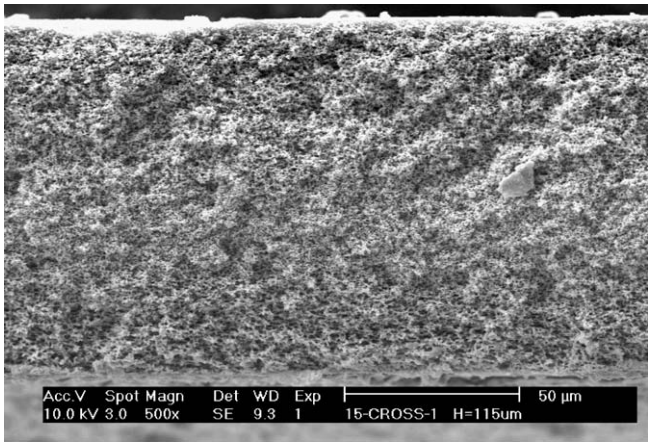

Fig. 1. SEM graph of the cross-section of a symmetric porous membrane.

The nominal operating conditions: fresh air inlet 35 °C and 0.021 kg/kg; exhaust air inlet 25 °C and 0.010 kg/kg. The corresponding inlet relative humidity (RH) is 59% and 51% for fresh air and exhaust air, respectively. During the experiment, air flow rate is changed by variable frequency pumps, to have different air velocities. Humidity, temperature, and volumetric flow rates are monitored at the inlet and outlet of the exchanger. To have a balanced flow, equal air flow rates are kept for the two air streams. Volumetric air flow rates are varied from 1.2 to 7.2 L/min, corresponding to air velocities from 0.5 to 3 m/s which are typical for commercial total heat mass exchangers. Air flow under such conditions is laminar, with Reynolds numbers not exceeding 500. The uncertainties are: temperature ±0.1 °C; humidity ±2%; volumetric flow rate ±1%. The final uncertainty for effectiveness and heat transfer coefficients is ±4.5%. The uncertainties of sensors are defined by the manufacturers. The uncertainties for the deduced value are estimated by uncertainty transfer equations, as introduced in [15,16].

2.2. Membrane materials

Industrial grade PVDF supplied by Guangzhou Tianma Co. Ltd. is used as the membrane raw material. The membrane is fabricated through following steps: (1) 15 g PVDF powder is weighted and placed into a vessel with 100 g *N*,*N*-dimethylformamide (DMF) at about 90 °C. The solution is heated and stirred until it is completely dissolved. It took about 2 h. (2) 3 g polyethylene glycol (PEG) and

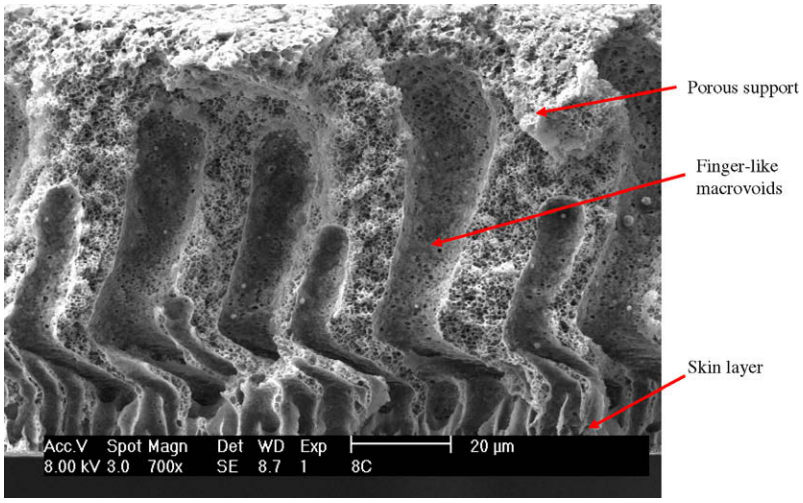

Fig. 2. SEM graph of the cross-section of an asymmetric porous membrane.

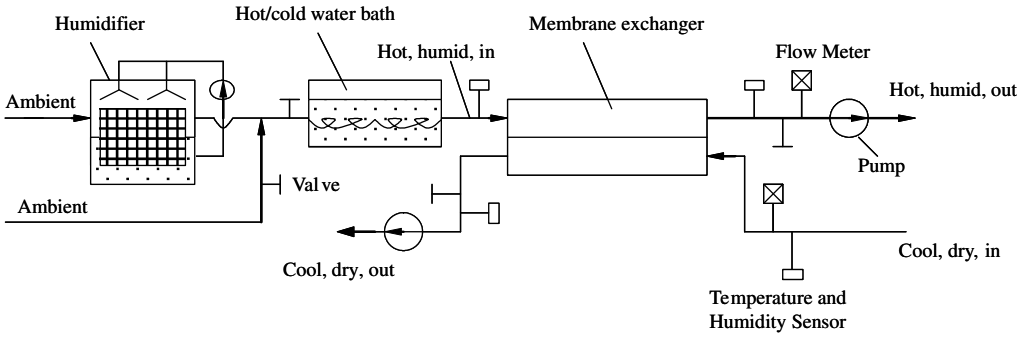

Fig. 3. A schematic of the test rig.

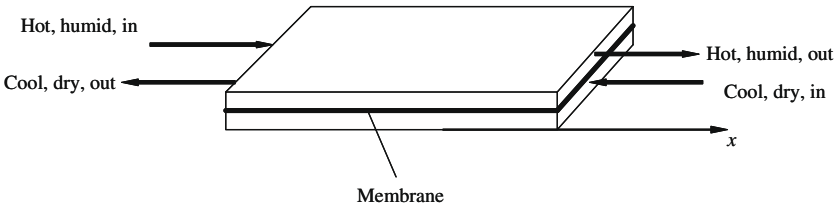

Fig. 4. Schematic of the counter flow heat mass membrane exchanger.

polyvinyl pyrrolidone (PVP) is added to the solution and kept stirring for another 2 h. (3) The solution is degassed and cast onto a clean glass plate with appropriate thickness control by a knife edge. (4) The glass with cast solution is dipped into a 25 °C water bath. Immediately, the solution solidifies and peels off the glass plate to form a membrane sheet. The membrane is soaked in water bath for 24 h for solvent and non-solvent exchange. (5) The membrane is dried in a vacuum drying box for 10 h. (6) The membrane is ready for structural characterization. The detailed fabrication and material modification processes are discussed elsewhere [17].

In order to observe the morphology of asymmetric flat sheet membranes just made, the dried membranes are broken in liquid nitrogen. Then the membrane samples are sputtered with a thin layer of gold using a SPI-Module sputter coater. The cross-section and surface of the flat sheet membranes are examined using a Joel JSM-5310V scanning microscope (SEM).

Fig. 5 shows the SEM graph of the cross-section of the PVDF membrane just made. As seen, it is a typical asymmetric membrane with finger-like macrovoids. The SEMs of the surface of the skin layer and the surface of the porous support layer are shown in Figs. 6 and 7, respectively.

3. Governing equations

3.1. Heat and mass diffusion through membrane

3.1.1. Effective gas diffusivity

The membrane structure is schematically depicted in Fig. 8. It is composed of three layers: a sponge-like porous layer, a sponge layer with finger-like macrovoids, and a skin layer. Their dimensions are plotted in the figure. Though the macrovoids may have differences, more or less, in length and dimension, in the model, they are approximated as identical cylinders, to ease the mathematical analysis. To account for their zigzag nature, a tortuosity is used later to compensate this feature.

Heat and moisture diffusion through the membrane can be depicted in Fig. 9. The established theory of gas diffusion in porous media considers three mechanisms: Poiseuille flow, Knudsen

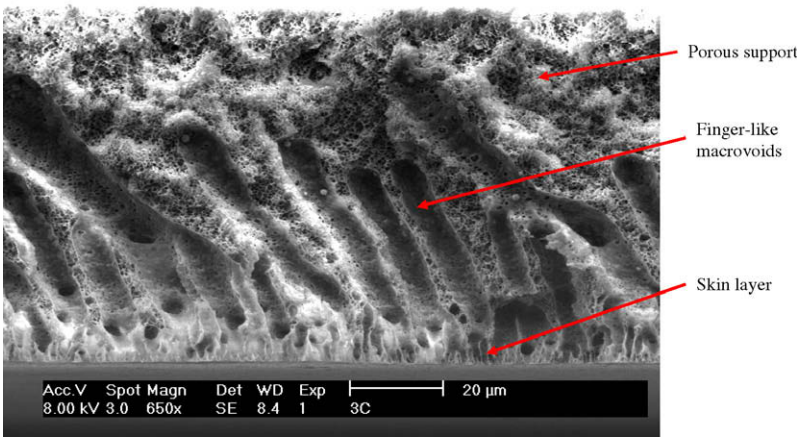

Fig. 5. SEM graph of the cross-section of the PVDF membrane used.

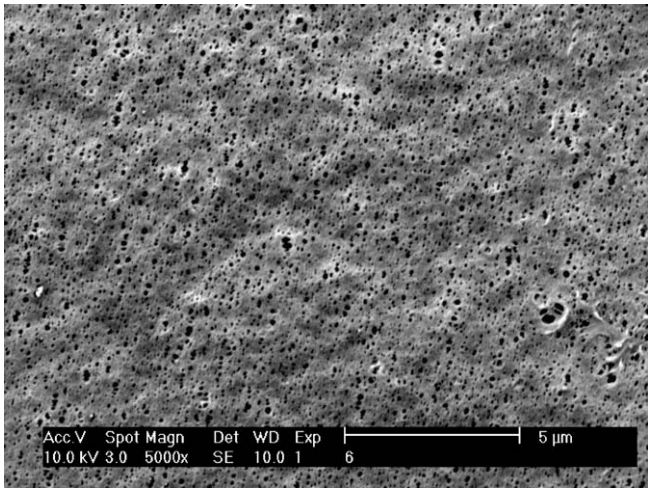

Fig. 6. SEM graph of the surface of the skin layer of the PVDF membrane used.

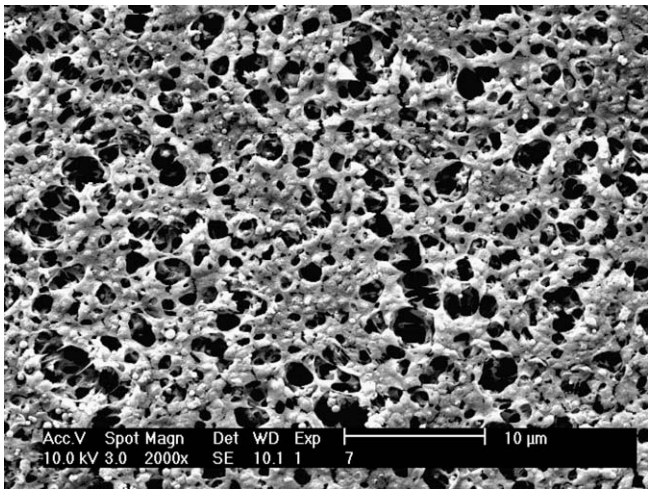

Fig. 7. SEM graph of the surface of the porous support layer of the PVDF membrane used.

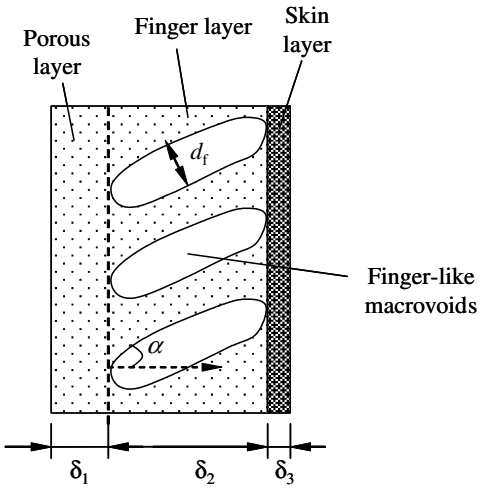

Fig. 8. Simplified structure of a finger-like macrovoids asymmetric membrane.

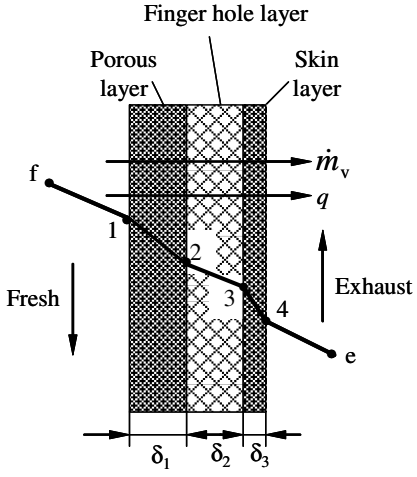

Fig. 9. Heat and mass transfer model in the asymmetric membrane.

diffusion, and/or a combination of them [18–21]. Viscous Poiseuille flow is bulk, non-separating flow caused by total pressure gradients, while in the Knudsen regime the transport is controlled by molecule–wall collisions, so that the molecules travel independently from each other. In contrary, molecule–molecule collisions define the molecular (ordinary) diffusion. In this study, due to the balanced flow, there is no transmembrane total pressure difference, so there is no bulk viscous Poiseuille flow. The mechanism for gas diffusion is combined Knudsen and ordinary diffusion. Under this mechanism, the diffusivity is given by [19]

$$D_{KO}^{-1} = \left(D_K^{-1} + D_O^{-1}\right)^{-1} \tag{1}$$

where the Knudsen diffusivity is [18]

$$D_K = \frac{d_p}{3}\sqrt{\frac{8RT}{\pi}M_v} \tag{2}$$

where d_p is mean pore diameter (m), T is temperature in K, M_v is the molecule weight of vapor (kg/mol); R is gas constant, 8.314 J/(mol K).

Ordinary diffusivity of water vapor molecule in air is expressed by [20]

$$D_0 = \frac{C_a T^{1.75}}{P_m\left(v_v^{1/3} + v_a^{1/3}\right)^2}\sqrt{\frac{1}{M_v} + \frac{1}{M_a}} \tag{3}$$

where $C_a = 3.203 \times 10^{-4}$. The terms v_v and v_a are molecular diffusion volumes and are calculated by summing the atomic contributions: $v_a = 20.1$, and $v_v = 12.7$. P_m is the mean total pressure within the membrane pores (Pa). M_a is molecular weight of air in kg/mol. M is 0.018 kg/mol for water vapor and 0.029 kg/mol for air, respectively.

Effective diffusivity for the sponge-like layer

$$D_{e1} = \frac{\varepsilon_1 D_1}{\tau_1} \tag{4}$$

where τ_1 and ε_1 are tortuosity and porosity of the first layer, respectively. Gas diffusivity D_1 is calculated by Eq. (1), based on the mean pore diameter in this layer.

Generally, resistance model is convenient in calculating heat mass transfer through a multi-component media. Gas diffusion through the asymmetric membrane can be depicted by the resistance model as shown in Fig. 10.

The gas diffusion resistance in the first layer is (s/m)

$$R_1 = \frac{\delta_1}{D_{e1}} \tag{5}$$

The resistance through the second layer comprises of two parallel parts: the finger-like macrovoids and the sponge-like micropores. The resistance through the finger-like macrovoids

$$R_{2f} = \frac{\tau_{2f} l_f}{\varepsilon_{2f} D_{2f}} \tag{6}$$

where τ_{2f} is the tortuosity of finger-like macrovoids in the second layer. For straight capillaries, tortuosity value is 1.0, for rather zigzag channels, tortuosity is always given a value of 3.0. In the equation, l_f is the length of macrovoids and is calculated by

$$l_f = \frac{\delta_2}{\cos\alpha} \tag{7}$$

where α is the skew angle of the finger-like macrovoids as depicted in Fig. 8. Porosity of finger-like macrovoids in the second layer, ε_{2f}, is defined as the ratio of total macrovoids area to membrane surface area by

$$\varepsilon_{2f} = \frac{n_f d_f}{\cos\alpha} \tag{8}$$

where n_f is the number of finger-like macrovoids per unit membrane length (1/m); d_f is the mean diameter of finger-like macrovoids. Gas diffusivity through macrovoids D_{2f} in Eq. (6) is calculated by Eq. (1), by substituting macrovoid mean diameter d_f as the character pore size.

Though the shapes and lengths of the macrovoids in a membrane may be different from each other, more or less, to simply the analysis, it is assumed that the finger-like macrovoids have the same cylindrical dimensions and are in parallel.

Besides gas diffusion through macrovoids, there is still some diffusion through the residual sponge-like micropores in this layer. The resistance through this part is

$$R_{2s} = \frac{\tau_1 \delta_2}{\varepsilon_1(1-\varepsilon_{2f})D_1} \tag{9}$$

where in the equation, the tortuosity, porosity, and diffusivity are considered as the same as the first layer, since they are similar in structure from SEM observations. The finger-like macrovoids walls has the same structure as the porous substrate.

The total resistance for this finger-like layer is the parallel of finger part and porous part

$$R_2 = \left(R_{2f}^{-1} + R_{2s}^{-1}\right)^{-1} \tag{10}$$

Effective diffusivity

$$D_{e2} = \frac{\delta_2}{R_2} \tag{11}$$

Total porosity for the second layer

$$\varepsilon_2 = \varepsilon_{2f} + \varepsilon_1(1-\varepsilon_{2f}) \tag{12}$$

Effective diffusivity for the third layer, i.e., the skin layer, is

$$D_{e3} = \frac{\varepsilon_3 D_3}{\tau_3} \tag{13}$$

where τ_3, δ_3, and ε_3 are tortuosity, thickness, and porosity of the third layer, respectively. Similarly, gas diffusivity in the third layer D_3 is calculated by Eq. (1), based on mean pore diameters in this layer.

Gas diffusion resistance in the skin layer is

$$R_3 = \frac{\delta_3}{D_{e3}} \tag{14}$$

According to Fig. 10, the total resistance for membrane

$$R_m = R_1 + R_2 + R_3 \tag{15}$$

Effective mass diffusivity through the whole membrane

$$D_{eff} = \frac{\delta_1 + \delta_2 + \delta_3}{R_m} \tag{16}$$

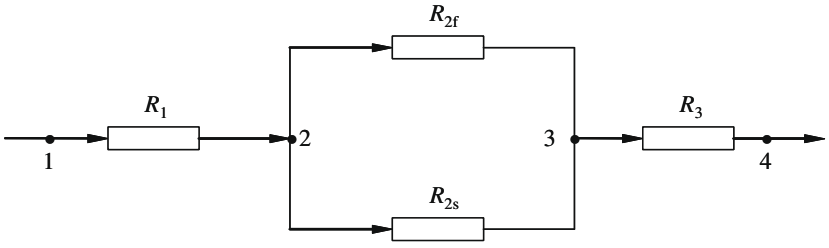

Fig. 10. Resistance model in the asymmetric membrane.

3.1.2. Effective thermal conductivity

Heat conductivity in the first layer can be analyzed by [22]

$$\lambda_1 = \lambda_a \varepsilon_1 + \lambda_s(1-\varepsilon_1) \tag{17}$$

where subscripts 'a' and 's' denote moist air and solid material part, respectively.

In the second layer, considering the media having a porosity of ε_{2f}, and a solid part heat conductivity of λ_1, a form similar to Eq. (17) can be used

$$\lambda_2 = \lambda_a \varepsilon_{2f} + \lambda_1(1-\varepsilon_{2f}) \tag{18}$$

Similarly, heat conductivity in the third layer can be expressed by

$$\lambda_3 = \lambda_a \varepsilon_3 + \lambda_s(1-\varepsilon_3) \tag{19}$$

Effective thermal conductivity

$$\lambda_{eff} = \frac{\delta_1+\delta_2+\delta_3}{\delta_1/\lambda_1+\delta_2/\lambda_2+\delta_3/\lambda_3} \tag{20}$$

It should be noted that membrane thermal resistance is rather smaller than boundary resistance on membrane two surfaces, due to the small thickness of membranes.

3.2. Coupled heat mass transfer in air streams

Two air streams, one hot and humid (fresh flow), and the other cool and dry (exhaust flow), exchange both sensible heat and moisture simultaneously in the exchanger in a counter flow arrangement, as has previously described in Fig. 4. Due to symmetry, a one-dimensional heat mass transfer model can be setup to govern the energy and mass conservations in the two air streams:

$$\frac{dT_f^*}{dx^*} = NTU_{sf}\left(T_{sf}^* - T_f^*\right) - q_{vf} \tag{21}$$

$$\frac{dT_e^*}{dx^*} = -NTU_{se}\left(T_{se}^* - T_e^*\right) - q_{ve} \tag{22}$$

$$\frac{d\omega_f^*}{dx^*} = NTU_{Lf}\left(\omega_{sf}^* - \omega_f^*\right) \tag{23}$$

$$\frac{d\omega_e^*}{dx^*} = -NTU_{Le}\left(\omega_{se}^* - \omega_e^*\right) \tag{24}$$

where x is flow direction for fresh stream. The exhaust air flows along $-x$-direction. In the energy equations (21) and (22), q_v is considered as the dimensionless enthalpy change induced by the moisture emission from the fresh to the exhaust as

$$q_{vf} = \frac{\dot{m}_v T_m^* c_{pv} x_F}{\rho_a H_d u_a (c_{pa} + \omega_f c_{pv})} \tag{25}$$

$$q_{ve} = \frac{\dot{m}_v T_m^* c_{pv} x_F}{\rho_a H_d u_a (c_{pa} + \omega_e c_{pv})} \tag{26}$$

where T_m^* is the dimensionless membrane mean temperature, c_p is specific heat (kJ kg^{-1} K^{-1}), subscripts a, v, e, f, and s refer to air, vapor, exhaust, fresh, and surface, respectively. In the equation, $\dot{m}_v$ is the moisture emission (or permeation) rate through membrane (kg m^{-2} s^{-1}), and is calculated by

$$\dot{m}_v = \rho_a \frac{\omega_f - \omega_e}{R_{tot}} \tag{27}$$

where the total resistance for moisture transfer, including convective resistance in two boundary layers, is

$$R_{tot} = \frac{1}{k_f} + R_m + \frac{1}{k_e} \tag{28}$$

In Eqs. (21)–(24), the effect of axial fluid conduction/diffusion is neglected. It is totally negligible for Pe (Peclet number) greater than 100, and is quite small even for $Pe = 10$. In practical applications axial conduction/diffusion is frequently of considerable significance for laminar flow of liquid metals, which have very low Prandtl numbers. For gases axial conduction/diffusion can be of importance only at extremely low Reynolds numbers [22].

The dimensionless temperature and humidity are defined by

$$T^* = \frac{T - T_{ei}}{T_{fi} - T_{ei}} \tag{29}$$

$$\omega^* = \frac{\omega - \omega_{ei}}{\omega_{fi} - \omega_{ei}} \tag{30}$$

The dimensionless coordinate is defined by

$$x^* = \frac{x}{x_F} \tag{31}$$

where x_F is channel length (m). The air side number of transfer units for heat and moisture are defined by

$$NTU_{sf} = \frac{h_f x_F}{\rho_a H_d u_a (c_{pa} + \omega_f c_{pv})} \tag{32}$$

$$NTU_{se} = \frac{h_e x_F}{\rho_a H_d u_a (c_{pa} + \omega_e c_{pv})} \tag{33}$$

$$NTU_{Lf} = \frac{k_f x_F}{u_a H_d} \tag{34}$$

$$NTU_{Le} = \frac{k_e x_F}{u_a H_d} \tag{35}$$

where k and h are convective mass transfer coefficient (m/s) and convective heat transfer coefficient (kW m^{-2}s^{-1}), respectively; u_a is air bulk velocity (m/s); H_d is channel height (m) as depicted in Fig. 3.

The outlet temperature and humidity values are calculated by Eqs. (21)–(24). Then it is convenient to convert humidity ratio to RH (relative humidity) with help from psychrometric chart. Outlet temperature and RH are two parameters that can be directly measured in experiment.

The convective heat transfer coefficient and mass transfer coefficient can be calculated by

$$Nu = \frac{hD_h}{\lambda_a} \tag{36}$$

$$Sh = \frac{kD_h}{D_O} \tag{37}$$

where D_h is the hydrodynamic diameter (m). For fully developed laminar flow in parallel plates channels, $Nu = 7.54$.

Convective mass transfer can be an analogy to convective heat transfer by [23]

$$Sh = Nu \cdot Le^{-1/3} \tag{38}$$

where Le is the Lewis number, which is 1.12–1.14 for moisture air.

3.3. Boundary and interface conditions

Fresh:

$$T_f^*\big|_{x^*=0} = 1 \tag{39}$$

$$\omega_f^*\big|_{x^*=0} = 1 \tag{40}$$

Exhaust:

$$T_e^*\big|_{x^*=1} = 0 \tag{41}$$

$$\omega_e^*\big|_{x^*=1} = 0 \tag{42}$$

The heat and moisture couplings between the air streams and the membrane surfaces are:

$$h_f(T_f - T_{sf}) = \frac{\lambda_{eff}}{\delta_{tot}}(T_{sf} - T_{se}) \tag{43}$$

$$h_e(T_{se} - T_e) = \frac{\lambda_{eff}}{\delta_{tot}}(T_{sf} - T_{se}) \tag{44}$$

$$k_f(\omega_f - \omega_{sf}) = \frac{D_{eff}}{\delta_{tot}}(\omega_{sf} - \omega_{se}) \quad (45)$$

$$k_e(\omega_{se} - \omega_e) = \frac{D_{eff}}{\delta_{tot}}(\omega_{sf} - \omega_{se}) \quad (46)$$

where δ_{tot} is the total thickness of membrane, i.e., the sum of three layers.

Heat flux (W/m^2) through membrane can be calculated by

$$q = \frac{\omega_f - \omega_e}{1/h_f + \delta_{tot}/\lambda_{tot} + 1/h_e} \quad (47)$$

4. Results and discussion

4.1. Solution procedure

A finite difference technique is used to discrete the partial differential equations developed for the air streams. The calculating domain is divided into a number of discrete nodes. Each node represents a control volume. The number of calculating node is 50 in x-direction. An upstream differencing scheme is used for two air streams. The two air streams and the asymmetric membrane are closely coupled. Heat transfer and mass transfer are also related to each other. Therefore, iterative techniques are needed to solve these equations. A description of the iterative procedure is as following:

(a) Calculate membrane gas diffusivity and heat conductivity parameters.
(b) Assume initial temperature and humidity fields in the two streams.
(c) Calculate the temperature and humidity values on membrane surfaces by Eqs. (43)–(46).
(d) Taking the current values of temperature and humidity on membrane surfaces as the default values, get the temperature and humidity profiles in two air streams by solving Eqs. (21)–(24).
(e) Go to (c), until the old values and the newly calculated values of temperature and humidity at all calculating nodes are converged.

After these procedures, all the governing equations are solved simultaneously. To assure the accuracy of the results presented, numerical tests were performed for the duct to determine the effects of the grid size. It indicates that 50 grids are adequate (less than 0.1% difference compared with 80 grids). The final numerical uncertainty is 0.1%.

The characterized membrane parameters and the exchanger geometry needed in the calculation are listed in Table 1. SEM graphs provide a basis for analysis. As seen, the mean diameter of the finger-like voids is 8.1 μm, around 10 times larger than pores in support layer. The density of finger voids is 70,000 per meter length.

The measured outlet temperature and relative humidity under various air flow rates are plotted in Figs. 11 and 12, respectively. In the figures, the measured values are denoted as the discrete dots. The calculated values from the above model are plotted in the figure as solid lines. Generally the model predictions are acceptable. The maximum deviations are 9.6% for temperature prediction, and 10.2% for relative humidity prediction. The deviations under small air flow rates are larger than those under higher air flow rates, due to the higher heat dissipation ratio to surroundings.

Table 1
Characterization of parameters of the asymmetric membrane developed

Symbol	Unit	Value	Symbol	Unit	Value
δ_1	μm	28	ε_1		0.65
δ_2	μm	45	ε_3		0.35
δ_3	μm	2.1	τ_1		3.0
d_{p1}	μm	0.72	τ_{2f}		1.0
d_{p3}	μm	0.17	τ_3		3.0
n_f	1/μm	0.07	α	deg	75
d_f	μm	8.1	x_F	mm	100
H_d	mm	2.0	λ_s	W m^{-1} K^{-1}	0.36
λ_a	W m^{-1} K^{-1}	0.0263			

4.2. Thermal and gas diffusion parameters

The calculated heat mass transfer parameters for membrane are listed in Table 2. The second layer has the highest gas diffusivity through a single pore or finger. This is because that the larger the pore (finger) diameter, the higher the gas diffusivity. Nevertheless, the diffusivity through a finger (D_{2f}) is in the same order with the diffusivity through a small pore (D_3). The effects of pore diameter on diffusivity are not obvious. However, due to the existence of straight finger voids, the total porosity in the second layer is greatly improved, and consequently the effective gas diffusivity through this layer (D_{2e}) is one order higher than that through the sponge support layer (D_{1e}). In one word, due to the increased porosity by straight finger voids, effective diffusivity can be greatly improved.

The total effective diffusivity is 1.23e−5 m^2/s. In contrast, if the membrane has no finger layer, the total effective diffusivity is 0.48e−5 m^2/s. As seen, the total mass transfer resistance is greatly decreased due to the existence of finger layers, by 1.6 times.

The calculated mass diffusion resistance is in agreement with above analysis. The first sponge layer has the highest resistance. Though the skin layer has the least amount of pores and the smallest pore diameters, due to the ultra-thin thickness, it has the least resistance. This indicates that for asymmetric membranes, the sponge-like layer has the largest mass transfer resistance.

Besides higher gas diffusivity, the parallel finger voids provide higher mechanical support for the membrane due to the honeycomb networking structure. Therefore, they are beneficial in industrial applications.

The higher the porosity is, the lower the thermal conductivity is. Table 2 shows that the calculated thermal conductivity is the least for the finger layer, which has the largest porosity. However, due to the small thickness of membrane, the final heat transfer resistance of the whole membrane is still negligible, comparing to the convective resistance in air boundary layers on two air streams. Therefore, the bad effects on heat transfer are not obvious.

4.3. Heat mass transfer in air streams

Temperature and humidity fields in the air streams are calculated for the nominal operating conditions and air velocity 1 m/s.

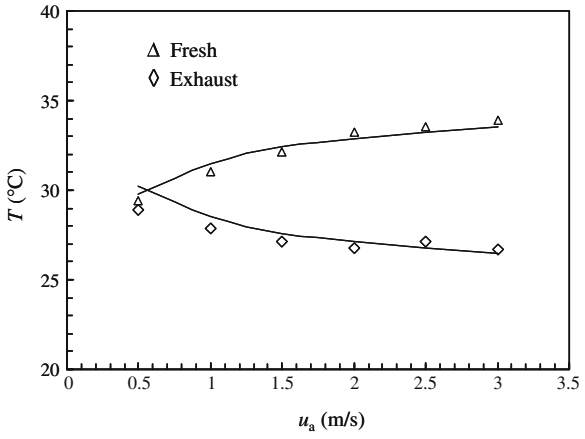

Fig. 11. Outlet temperature of the two air streams under various air flow rates, the solid lines are calculated, and the discrete dots are measured values.

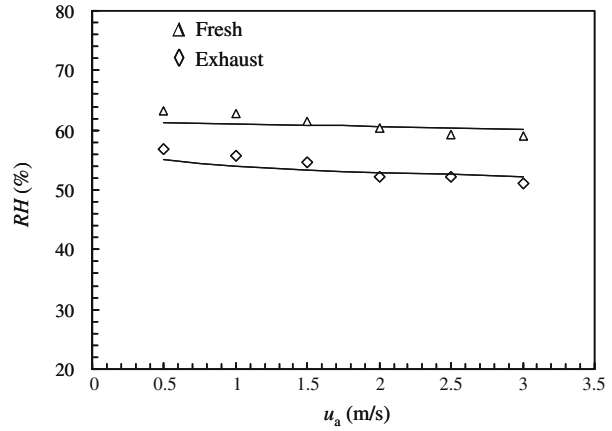

Fig. 12. Outlet relative humidity of the two air streams under various air flow rates, the solid lines are calculated, and the discrete dots are measured values.

Table 2
Calculated heat mass transfer parameters for membrane

Symbol	Unit	Value	Symbol	Unit	Value
D_1	10^{-5} m^2/s	2.35	D_{e1}	10^{-5} m^2/s	0.51
D_{2f}	10^{-5} m^2/s	2.77	D_{e2}	10^{-5} m^2/s	1.76
D_3	10^{-5} m^2/s	1.53	D_{e3}	10^{-5} m^2/s	0.18
ε_1		0.65	R_1	s/m	5.49
ε_2		0.87	R_2	s/m	2.55
ε_3		0.35	R_3	s/m	1.17
λ_1	W m^{-1} K^{-1}	0.1431	λ_2	W m^{-1} K^{-1}	0.0702
λ_3	W m^{-1} K^{-1}	0.2432			

The dimensionless temperature and humidity profiles for the two air streams are shown in Fig. 13.

As seen from this figure, the temperature of fresh air decreases along the flow in x-direction, while the temperature of the exhaust increases along the flow in $-x$-direction, because the two flows are in counter flow arrangement. Similar trends are found for humidity profiles. Further, the mass transfer resistance for membrane is larger than heat transfer resistance, so the temperature changes more quickly than humidity does. In summary, heat is more effectively exchanged than moisture is.

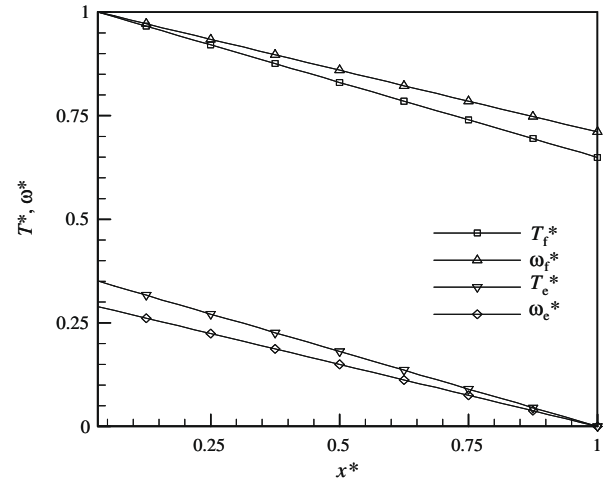

Fig. 13. Local dimensionless temperature and humidity variations along flow.

The mean heat flux and moisture permeation rate through the membrane are shown in Fig. 14 under various air flow velocities. As seen, the higher the bulk air velocity, the higher the heat flux and mass permeation rates. The reason behind is that the higher the air velocity, the lower the boundary layer resistance on air sides. Heat flux can be as high as 200 W/m^2, and gas permeation can be as high as 1.8×10^{-4} kg m^{-2} s^{-1}, indicating high heat mass exchanger potentials with such porous membranes.

5. Conclusions

Finger-like macrovoids membranes are the most important membranes for industrial use. To build relations between heat mass transfer properties and the unique microstructures inside is a challenging work. This study addressed the task by characterization of membrane microstructures and the analysis of various resistances. The dimensions of finger-like voids are classified to setup the thermal and gas diffusion model. Temperature and humidity profiles in a membrane exchanger are numerically obtained. the heat and mass transfer performance is then investigated. The results found as follows:

(1) Due to the existence of 70,000 straight finger voids per 1 m membrane length, the total porosity in the membrane is greatly improved. The final effective gas diffusivity through the finger layer is one order higher than that through the sponge support layer.
(2) Though the skin layer has the least amount of pores and the smallest pore diameters, due to the ultra-thin thickness, it has the least resistance. For asymmetric membranes, the sponge-like layer has the largest mass transfer resistance.
(3) The calculated thermal conductivity is the least for the finger layer. However, due to the small thickness of whole membrane, the bad effects of increased voids on heat transfer are not obvious.
(4) Above transport analysis discloses that an ideal membrane structure desires straight, parallel, vertical, big finger holes. Besides, both the porous substrate and the skin layer should be as thin as possible. From these perspectives, the current membrane making process needs further optimization. Besides instantaneous demixing, composition of the cast solution should be further optimized.

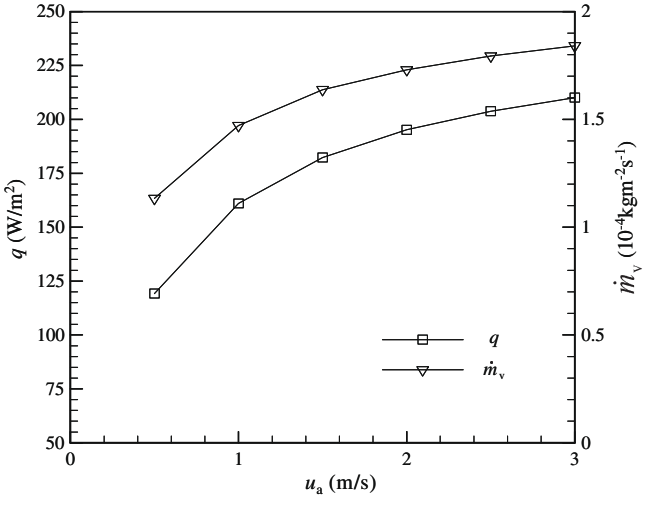

Fig. 14. Variations of heat flux and moisture permeation rate through the membrane.

Acknowledgements

This Project 50676034 is supported by National Natural Science Foundation of China. The project is also supported by the National High Technology Research and Development Program of China (863), 2008AA05Z206; and National Key Project of Scientific and Technical Supporting Programs, No. 2006BAA04B02.

References

[1] L. Martinez, J.M. Rodriguez-Maroto, On transport resistances in direct contact membrane distillation, J. Membrane Sci. 295 (1–2) (2007) 28–39.
[2] A.M. Alklaibi, N. Lior, Heat and mass transfer resistance analysis of membrane distillation, J. Membrane Sci. 282 (1–2) (2006) 362–369.
[3] E. Favre, Temperature polarization in pervaporation, Desalination 154 (2) (2003) 129–138.
[4] F. Roa, J.D. Way, R.L. McCormick, S.N. Paglieri, Preparation and characterization of Pd—Cu composite membranes for hydrogen separation, Chem. Eng. J. 93 (1) (2003) 11–22.
[5] C. Fukuhara, A. Igarashi, Two-dimensional simulation of a membrane reactor for dehydrogenation of ethylbenzene, considering heat mass transfer, J. Chem. Eng. Jpn. 36 (5) (2003) 530–539.
[6] A. Hussain, A. Seidel-Morgenstern, E. Tsotsas, Heat and mass transfer in tubular ceramic membranes for membrane reactors, Int. J. Heat Mass Transfer 49 (2006) 2239–2253.
[7] J.K. Kuo, C.K. Chen, The effects of buoyancy on the performance of a PEM fuel cell with a wave-like gas flow channel design by numerical investigation, Int. J. Heat Mass Transfer 50 (21–22) (2007) 4166–4179.
[8] L.Z. Zhang, Heat and mass transfer in a cross-flow membrane-based enthalpy exchanger under naturally formed boundary conditions, Int. J. Heat Mass Transfer 50 (21–22) (2007) 151–162.
[9] K.R. Kistler, E.L. Cussler, Membrane modules for building ventilation, Chem. Eng. Res. Des. 80 (2002) 53–64.
[10] J.Z. Ren, Z.S. Li, F.S. Wong, Membrane structure control of BTDA-TDI/MDI (P84) co-polyimide asymmetric membranes by wet-phase inversion process, J. Membrane Sci. 241 (2004) 305–314.
[11] S. Atchariyawut, C.S. Feng, R. Wang, R. Jiraratanon, D.T. Liang, Effect of membrane structure on mass transfer in the membrane gas–liquid contacting process using microporous PVDF hollow fibers, J. Membrane Sci. 285 (2006) 272–281.
[12] M. Wang, L.G. Wu, J.X. Mo, C.J. Gao, The preparation and characterization of novel charged polyacrylonitrile/PES-C blend membranes used for ultrafiltration, J. Membrane Sci. 274 (2006) 200–208.
[13] R.X. Liu, X.Y. Qiao, T.S. Chung, Dual-layer P84/polyethersulfone hollow fibers for pervaporation dehydration of isopropanol, J. Membrane Sci. 294 (1–2) (2007) 103–114.
[14] N. Scharnagl, H. Buschatz, Polyacrylonitrile (PAN) membranes for ultra- and microfiltration, Desalination 139 (1–3) (2001) 191–198.
[15] Y.P. Zhang, Y. Jiang, L.Z. Zhang, Y.C. Deng, Analysis of thermal performance and energy saving effect of membrane-based Heat Recovery Ventilator, Energy 25 (2000) 515–527.
[16] S.T. Kline, F.A. Mcclintock, Describing uncertainties in single-sample experiments, Mech. Eng. 75 (1953) 3–8.
[17] L.Z. Zhang, Y.Y. Wang, C.L. Wang, H. Xiang, Synthesis and characterization of a PVA/LiCl blend membrane for air dehumidification, J. Membrane Sci. 308 (2008) 198–206.
[18] E.L. Cussler, Diffusion-Mass Transfer in Fluid Systems, Cambridge University Press, Cambridge, 2000.
[19] L.Z. Zhang, Mass diffusion in a hydrophobic membrane humidification/dehumidification process: the effects of membrane characteristics, Separ. Sci. Technol. 41 (8) (2006) 1565–1582.
[20] M. Tomaszewska, M. Gryta, A.W. Morawski, Mass transfer of HCl and H_2O across hydrophobic membrane during membrane distillation, J. Membrane Sci. 166 (2000) 149–157.
[21] Jianyin Xiong, Yinping Zhang, Xinke Wang, Dongwu Chang, Macro-meso two scale model for predicting the VOC diffusion coefficients and emission characteristics of porous building materials, Atmos. Environ. 42 (2008) 5278–5290.
[22] A.K. Datta, Porous media approaches to studying simultaneous heat and mass transfer in food processes. I. Problem formulations, J. Food Eng. 80 (2007) 80–95.
[23] J.L. Niu, L.Z. Zhang, Membrane-based enthalpy exchanger: material considerations and clarification of moisture resistance, J. Membrane Sci. 189 (2001) 179–191.